

GCM SIMULATIONS OF UNSTABLE CLIMATES IN THE HABITABLE ZONE

ADIV PARADISE¹ AND KRISTEN MENU^{1,2}

¹*Department of Astronomy and Astrophysics, University of Toronto, St. George*

²*Centre for Planetary Sciences, Department of Physical and Environmental Sciences, University of Toronto, Scarborough*

Submitted to The Astrophysical Journal

ABSTRACT

It has recently been proposed that Earth-like planets in the outer regions of the habitable zone experience unstable climates, repeatedly cycling between glaciated and deglaciated climatic states (Menou 2015). While this result has been confirmed and also extended to explain early Mars climate records (Haqq-Misra et al. 2016; Batalha et al. 2016), all existing work relies on highly idealized zero-dimensional climate models. Here, we confirm that the phenomenology of climate cycles remains in 3D Earth climate models with considerably more degrees of freedom. To circumvent the computational barrier of integrating climate on Gyr timescales, we design a hybrid 0D-3D integrator which uses a general circulation model (GCM) as a short relaxation step along a long evolutionary climate sequence. We find that GCM climate cycles are qualitatively consistent with reported zero-dimensional results. This establishes on a firmer ground the notion that outer habitable zone planets may be preferentially found in transiently glaciated states.

Keywords: planets and satellites: terrestrial planets, planets and satellites:
atmospheres, methods: numerical, astrobiology

I. INTRODUCTION

Recent estimates of the habitable zone place an inner edge at 0.99 AU and an outer edge at 1.7 AU (Kopparapu et al. 2013). However, these estimates come from 1D climate models which only consider equilibria on short timescales. That short-term equilibrium comes from an energy balance requirement—the heat released into space must balance the net solar radiation (insolation) received from the sun North et al. (1981). We refer to this as thermal equilibrium. Planets can also demonstrate stability or instability on longer timescales. Changes in glaciation or greenhouse gases over time can alter the planet’s albedo and outgoing thermal emission, affecting the thermal equilibrium temperature (North et al. 1981; Pierrehumbert 2005). It may be that a more realistic habitable zone that takes into account long-term stability will be significantly more constrained. The emergence of complex life depends as much on the long-term stability of a habitable climate as it does on its immediate habitability—an informed search for Earth analogs thus depends strongly on understanding climate variation throughout the habitable zone.

A planet’s climate stability can be tied to the carbon-silicate cycle. On planets containing land plants, weathering is decoupled from the CO_2 partial pressure (hereafter pCO_2) by biological activity (Pierrehumbert 2010; Schwartzman & Volk 1989). However, on planets lacking land plants, the carbon cycle acts as a thermostat—increased temperatures or pCO_2 surpluses lead to increased weathering and CO_2 sequestration, while a deficit reduces weathering, allowing volcanic outgassing to replenish CO_2 (Pierrehumbert 2010; Walker et al. 1981; Schwartzman & Volk 1989; Williams & Kasting 1997; Kump et al. 2000). The climate on such a planet tends toward an equilibrium point. At low insolation, the equilibrium point may be cold enough for total glaciation (Menou 2015; Pierrehumbert 2005; Hoffman et al. 1998). In this scenario, weathering ceases in the absence of liquid water, implying that no equilibrium can be reached. Volcanic outgassing continues, and at a certain point pCO_2 will be high enough for the ice to melt, resulting briefly in warm wet conditions, followed by rapid weathering and cooling. Thus, on geological timescales the climate may cycle between long snowball events and brief warm wet periods (Menou 2015). Evidence of glacial deposits at then-tropical latitudes on Earth has been linked to this hypothesis (Tajika 2007).

Menou (2015) used a zero-dimensional reduction of 1D models to approximate energy-balanced climates of Earth-like planets at varying orbital distances throughout the habitable zone. He found that climate cycles, wherein the planet oscillates between brief warm periods and long frozen periods, should dominate much of the outer habitable zone. However, 1D models lose inherently 3D phenomena, such as albedo variations, sea ice distributions, horizontal heat transport, air currents, etc. These phenomena can be captured with a 3D model, which is the topic of this study.

II. METHODS

II.A. *Simulating Long Timescales*

Since climate cycles, as observed in 1D models by [Menou \(2015\)](#) and [Haqq-Misra et al. \(2016\)](#), have periods of at minimum millions of years, the primary obstacle to simulating them in 3D models is the computational cost of millions of years or more of climate evolution in existing 3D models. PlaSim, the GCM used in this study, takes on the order of minutes of wall-time to compute one simulated year. Computing millions of years directly is thus unfeasible. A more detailed discussion of the computational cost of direct computation vs. our method is presented in [Appendix A](#). An approach is needed that allows a model to skip through millions of years of evolution, only computing a couple years at certain key points.

We achieve this by noting that the climate exhibits different types of equilibria, which operate on different timescales. Thermal equilibrium, when the planet exhibits a relatively unchanging seasonally-averaged global temperature, is achieved on the order of years to decades following a perturbation. Weathering equilibrium, on the other hand, when global outgassing and weathering rates cancel each other out and the global $p\text{CO}_2$ level is relatively constant, is achieved (if at all) on much longer geological timescales of millions of years. This latter timescale is many orders of magnitude longer than the thermal timescale, which means that weathering effects can typically be disregarded on thermal timescales, and vice versa. The CO_2 partial pressure is a global quantity, which means that only global, zero-dimensional terms are needed to compute its evolution. Thermal equilibrium, however, must be computed using a full 3D treatment to capture various mechanisms such as sea ice feedback, wind circulation, cloud formation, etc. The global weathering rate also depends on 3D features such as landmasses and ice caps. Therefore, we construct a hybrid 3D-0D model in which a full 3D model computes the evolution of a new thermal equilibrium following a 0D perturbation in $p\text{CO}_2$. We compute the size and duration of that perturbation by computing the global weathering rate from the results of the 3D model. This means that millions of years of evolution of slow change can instead be approximated by allowing the CO_2 partial pressure to change by an equivalent amount, and then allowing the climate to relax back to thermal equilibrium. In this way, we treat the GCM not as the primary driver of model evolution, but as a relaxation step in a simpler 0D model that controls the long-term model evolution.

For the 3D relaxation step, we use the Planet Simulator (PlaSim) developed at the Universität Hamburg, a 3D Earth-system general circulation model (GCM) developed for fast and easy study of Earthlike climate systems. PlaSim solves primitive equations for vorticity, temperature, divergence, and pressure using the spectral transform method. It includes a 50-meter mixed-layer slab ocean, thermodynamic sea ice, a bucket model of soil hydrology, moist and dry convection, interactive clouds, large-scale precipitation, and a parameterized longwave and shortwave radiation model ([Fraedrich et al. 2005](#)). It uses a latitude-longitude grid with an atmosphere discretized into multiple vertical levels. For a more complete description of the model, readers are referred to the PlaSim Reference Manual ([Lunkeit et al. 2012](#)).

Our weathering implementation is based on a parameterization of Earth’s silicate weathering in the absence of vascular land plants. We use the same form used in [Menou \(2015\)](#), which is a form of the parameterization described in [Berner \(2001\)](#). That parameterization is based on observations of cation concentrations in river runoff, laboratory measurements, and seafloor drill cores. Our functional weathering form is thus

$$\frac{W}{W_{\oplus}} = \left(\frac{p\text{CO}_2}{p\text{CO}_{2,\oplus}} \right)^{\beta} e^{[k_{\text{act}}(T_s - 288)]} [1 + k_{\text{run}}(T_s - 288)]^{0.65}, \quad (1)$$

where T_s is the surface temperature, $p\text{CO}_{2,\oplus}$ is the pre-industrial $p\text{CO}_2$ of 330 μbar , and W_{\oplus} is the weathering rate at $T_s = 288$ K. k_{act} is related to the chemical activation energy of the weathering reaction and is set to 0.09, and k_{run} is a runoff efficiency factor set to 0.045, which helps account for changes in precipitation. β is the dependence on $p\text{CO}_2$, and is set to 0.5 ([Menou 2015](#); [Pierrehumbert 2010](#); [Kump et al. 2000](#)). We follow a similar procedure to [Edson et al. \(2012\)](#) to compute this locally across the planet. When the planet is not in a snowball state, implying global mean temperatures above approximately 260 K, we evaluate [Equation 1](#) at each cell if the cell has land surface and has surface temperatures above 273.15 K, 4 times per simulated day in 6-hour intervals. The weathering rate is averaged over a full year in each cell, to compute a localized annual mean weathering rate. This is then spatially averaged over the globe to compute the annual mean global weathering rate.

We run PlaSim in the T21 configuration, with 64 latitudes and 32 longitudes. We use 10 vertical grid levels, turn on the mixed-layer ocean, and use a timestep of 45 minutes. We allow $p\text{CO}_2$ to change year-after-year according to the annual weathering and outgassing rates. This change is usually extremely small, but it costs nothing if we are already computing the weathering rate, and yields slightly more accuracy, particularly during episodes of very fast weathering when a planet has just emerged from a snowball state. We run PlaSim for a minimum of 11 years, at which point we use NumPy to perform a linear fit to the annual mean surface temperature. We average the slopes of fits for 9-year histories ending in each of the three most recent years to give a sense of the general trend of the past decade and to try to minimize the effect of outliers. If this average slope has an absolute value greater than 0.05 K/year, then we consider PlaSim to not have reached thermal equilibrium, and allow it to continue to run for one more year. This check is considered at the end of each simulated year. This procedure has been determined empirically to achieve approximate thermal equilibrium, and other methods for determining thermal equilibrium should work as well, achieving similar results.

The zero-dimensional $p\text{CO}_2$ -evolution component of the model is computed by solving

$$\frac{d}{dt} p\text{CO}_2 = V - W(T_s, p\text{CO}_2), \quad (2)$$

as in [Menou \(2015\)](#). We first compute the annual temperature change relative to the change in $p\text{CO}_2$ over the last two years of the simulation, $\partial T / \partial p\text{CO}_2$. Since the surface temperature is the quantity most directly related to sea ice extent, which determines the qualitative

model state, we aim to control the temperature evolution, rather than simply controlling the $p\text{CO}_2$ evolution. This is because sea ice extent and surface temperature become increasingly sensitive to perturbations in $p\text{CO}_2$ near the global freeze/thaw point. We therefore compute the $p\text{CO}_2$ step size as

$$\Delta p\text{CO}_2 = \text{sign}(V - W) \Delta T \frac{\partial p\text{CO}_2}{\partial T}, \quad (3)$$

where ΔT is the absolute value of the desired temperature change, V is the volcanic CO_2 outgassing rate, and W is the global CO_2 weathering rate. The weathering rate is only needed at this point to determine the sign of the change. In order to gain higher sampling resolution of the transitions between snowball and warm states, we decrease the temperature step size ΔT near the global freeze/thaw point. For temperatures between 240 and 268 K, we aim for a change of 0.5 K per step. For temperatures between 235–240 K and 268–273 K, we aim for 1 K per step. And for temperatures below 235 K or above 273 K, we aim for 2 K per step. We use finer sampling near the transition because a model with too-coarse sampling could artificially introduce climate cycles in models with weathering equilibrium temperatures near the global freeze/thaw point.

We can combine this $p\text{CO}_2$ step size with the $p\text{CO}_2$ rate of change at the end of the last model year to estimate the duration of the $p\text{CO}_2$ adjustment:

$$\Delta t = \frac{V - W}{\Delta p\text{CO}_2}. \quad (4)$$

Because this estimate uses only the $p\text{CO}_2$ rate of change at the end of the previous relaxation step, this method is likely not very accurate. However, for the purposes of identifying climate cycles and the order of magnitude of their timescales, this method is likely sufficient. A more robust and sophisticated technique could perhaps be used in its place to yield more accurate estimates of the period of a given cycle, but is beyond the scope of this paper.

II.B. *Establishing Limits on Climate Stability*

We further attempt to determine the limits of the temperate habitable zone, beyond which limit cycles should occur. We accomplish this with a parameter sweep, running PlaSim to thermal equilibrium for 31 different insolutions, ranging from $1.0 F_\oplus$ to $0.75 F_\oplus$, where F_\oplus is the incident solar flux received by the present-day Earth, taken here to be 1367 W m^{-2} . These insolutions correspond to orbital radii between 1 and 1.15 AU, separated by 0.005 AU. For each insolation, we prescribe a CO_2 partial pressure ranging from 0.1 μbars to 6 bars, separated by 0.1 dex, and run the model to thermal equilibrium for that given $p\text{CO}_2$ and insolation. At the transition points between snowball and temperate climates, we reduce the sample spacing to 0.01 dex. We do this for both warm, Earth-like initial conditions with only limited glaciation, and snowball initial conditions. We use Earth-like land distributions and orography. We compute the global weathering rate averaged over two decades for each model at thermal equilibrium. These values give an estimate of the edges of the temperate habitable zone in terms of outgassing rates and insolation.

III. RESULTS

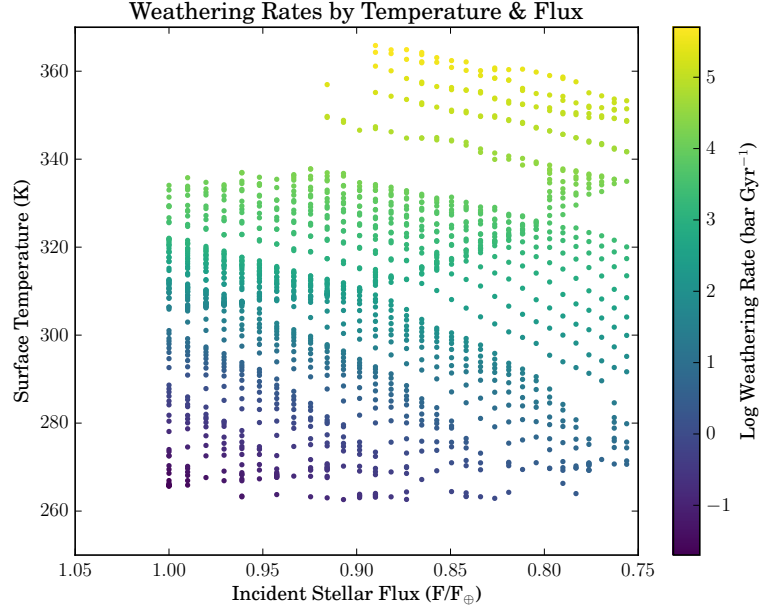
The parameter sweep, whose results are shown in [Figure 1](#), show a range of temperatures between roughly 250 and 265 K for which no equilibrated models are found. This is because in that temperature range, sensitive albedo feedbacks with sea ice lead to either rapid glaciation into a snowball state or a rapid thaw into a temperate state. The weathering rates at the lower limit of the partially-frozen models are therefore the minimum outgassing rates required to maintain stable temperate climates. These rates are shown in [Figure 2](#). The minimum outgassing rate is exponentially related to the insolation, such that

$$\frac{V}{V_{\oplus}} = \kappa e^{-\alpha \left(\frac{F}{F_{\oplus}} \right)}, \quad (5)$$

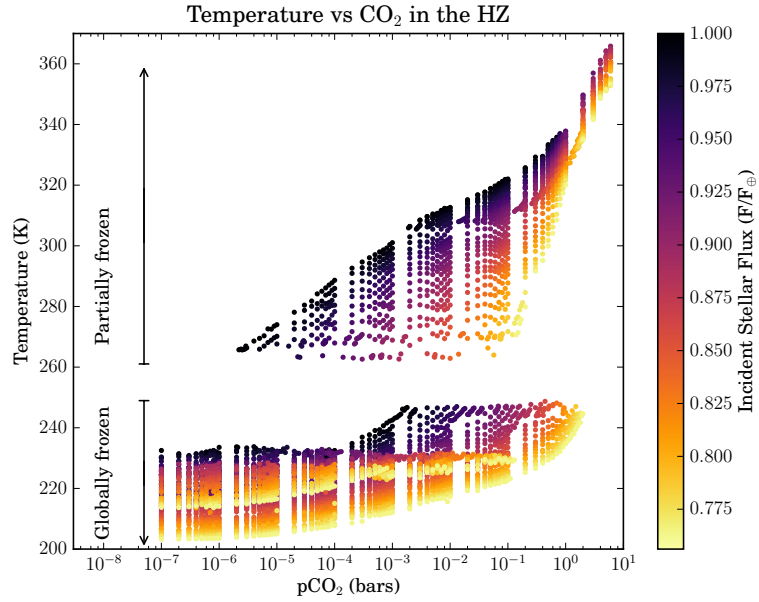
where κ and α are constants, and in our fit equal to approximately 3.6×10^7 and 23 respectively. This has a similar functional form to the limit of the temperate habitable zone derived by [Abbot \(2016\)](#). [Haqq-Misra et al. \(2016\)](#) argued that [Menou \(2015\)](#) used an inappropriate estimate of Earth’s outgassing rate, citing a more appropriate value of approximately 63 bars Gyr^{−1}. We test the model’s dependence on this by running the same models with 63 bars Gyr^{−1} as the Earth outgassing rate. The results are also shown in [Figure 2](#). Since the weathering parameterization, [Equation 1](#), uses values normalized to Earth, changing the Earth outgassing rate simply shifts the position of the parameter space, rather than changing its shape. The result is that climate cycles occur at outgassing rates approximately 10 times higher than suggested when assuming Earth outgasses 7 bars Gyr^{−1}.

Our hybrid 0D-3D models were run at $0.14 V_{\oplus}$, or 1 bar Gyr^{−1}, with 78%, 79%, and 80% F_{\oplus} , or 1067, 1079, and 1094 W m^{−2} insolation. We assume Earth obliquity and seasons, orbital eccentricity, land fraction, and continental distribution and orography. As expected, we find that these models have unstable climates characterized by limit cycling, as shown in [Figure 3](#). The cycles all have periods of approximately 1.3–1.6 Gyr. The warm periods last for 14 Myr, 12 Myr, and 13 Myr respectively, as shown in [Figure 4](#). The warm periods are therefore approximately 1% of the total cycle duration. It is also of note that the mean temperature and pCO₂ curves throughout the cycle have the same form as those identified in [Menou \(2015\)](#). Inconsistencies between different cycle periods are likely the result of imperfections in the pCO₂-stepping algorithm and estimation of the time intervals between data points. This may also explain why in this range of insolutions we do not observe a significant correlation between insolation and the fraction of the cycle spent in the temperate phase, as in [Menou \(2015\)](#)—our timestepping may not be precise enough to resolve that trend over small differences in insolation. With an improved model and algorithm for spanning these geological timescales, we expect greater consistency between cycles. Using the outgassing estimate in [Haqq-Misra et al. \(2016\)](#), we find that cycle periods decrease by roughly a factor of 10, consistent with a nearly factor of 10 increase in the speed at which atmospheric pCO₂ is replenished. These are consistent with the cycle periods found by [Abbot \(2016\)](#).

To probe the sensitivity to continental distribution, we run a set of models at Earth insolation and 1 mbar Gyr^{−1} outgassing. Each has the same land fraction as modern Earth, but the

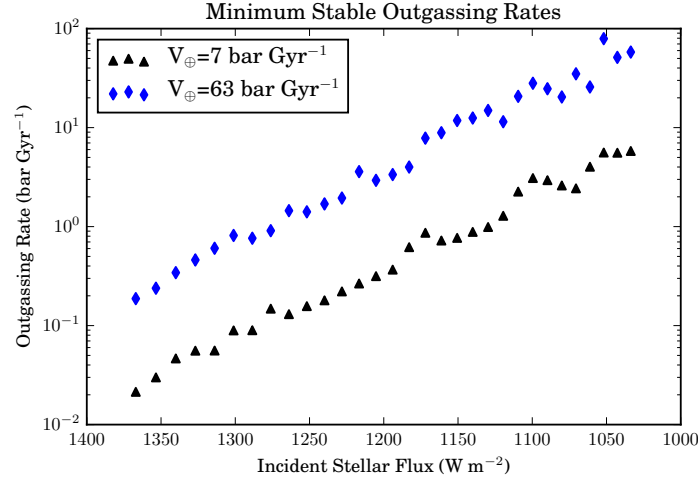


(a)

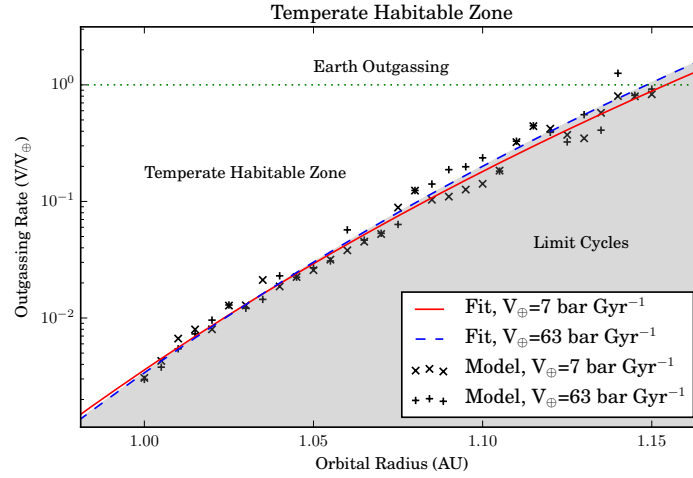


(b)

Figure 1. All models run in the parameter sweep, presented in two different ways. Each point represents the annual mean temperature of the last year of a model run to thermal equilibrium for a given CO_2 partial pressure and insolation. The figure in (a) shows the weathering rate at thermal equilibrium for each temperate climate, excluding models with no weathering (snowball states), and (b) shows the dependence on pCO_2 , which illustrates the insolation bistability proposed by [Budyko \(1969\)](#). No thermal equilibria exist for temperatures between approximately 250–260 K, due to an ice-albedo feedback process that is unstable to perturbations. Models on either side of this gap therefore represent the globally frozen states that comprise the majority of the cycle duration, and the partially frozen or globally warm states which punctuate the cycles. The weathering rates of the coldest models in (a) represent the minimum outgassing rates for temperate stability.



(a)



(b)

Figure 2. Minimum outgassing rates for stable temperate climates as a function of insolation (a) and the decomposition of the habitable zone into temperature and limit cycling regions (b). [Haqq-Misra et al. \(2016\)](#) suggested that 63 bars Gyr^{-1} may be a more appropriate estimate for Earth’s outgassing rate than the 7 bars Gyr^{-1} used in [Menou \(2015\)](#), so panel (a) compares the results of parameter sweeps done with each assumption. The result is a simple translation; since model weathering rates are calibrated to Earth’s outgassing rate, the only effect is on limit cycle timescales, rather than the overall prevalence of unstable climates. Both obey an exponential trend, such that $v = \kappa e^{-\alpha f}$, where the outgassing $v = V/V_{\oplus}$, and insolation $f = F/F_{\oplus}$. In this fit, $\kappa \approx 3.6 \times 10^7$, and $\alpha \approx 23$. Panel (b) shows the data (black) and fits (red and blue) for both assumptions, normalized to Earth in each case, showing the strength of the agreement. Therefore, the habitable zone can be divided into a temperate habitable zone, consisting of outgassing rates above the fit, and limit cycles beyond that. For current Earth, that suggests that the temperate habitable zone extends to approximately 1.14–1.15 AU.

land is distributed either in a rectangular supercontinent centered on the equator, a circular supercontinent centered on a pole, two circular continents centered on the poles, and three models with most land at the poles but with a small continent of varying size at the equator. Each model assumes flat orography for simplicity. Of these models, only the equatorial su-

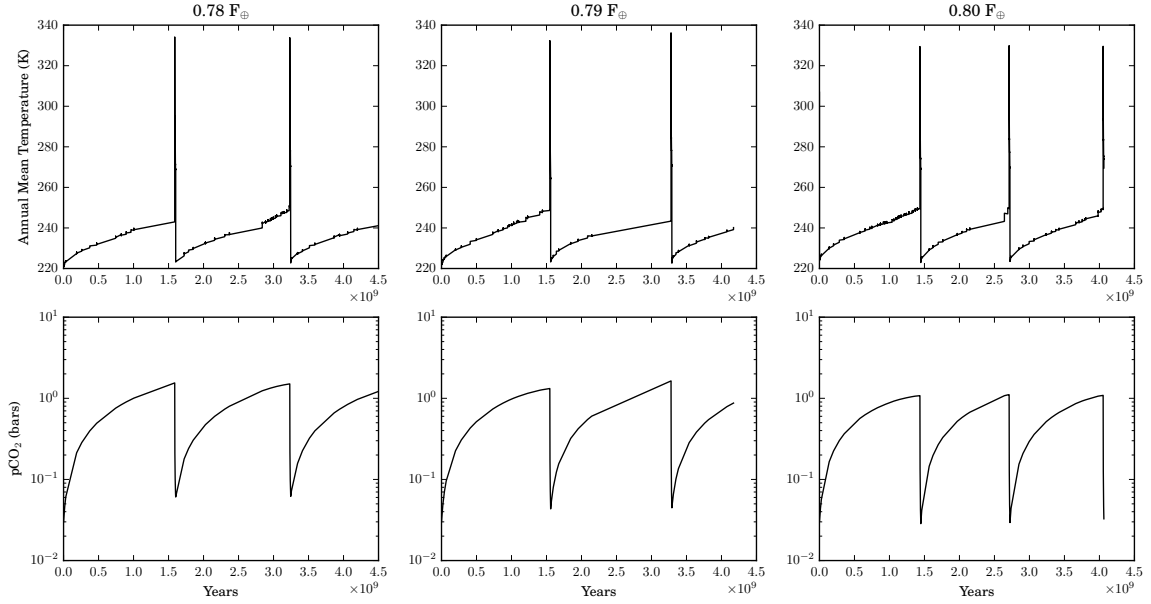
Climate Cycles, $V_{\oplus}=7$ bar/Gyr

Figure 3. The climate cycles observed at 0.78, 0.79, and 0.80 F_{\oplus} , with 0.14 V_{\oplus} . These insolation levels correspond to approximately 1.12, 1.125, and 1.13 AU in our own solar system. These parameters were chosen based on the weathering rates identified in Figure 2—at these outgassing rates, the temperature favored by weathering equilibrium is not a stable thermal state. The cycles have a period of approximately 1–1.5 Gyr, and the mean temperature and $p\text{CO}_2$ curves have the same form as those identified in lower-dimensional models in Menou (2015); Haqq-Misra et al. (2016). The cycle periods decrease by roughly a factor of 10 if Earth is assumed to have a higher outgassing rate, as in Haqq-Misra et al. (2016) and Abbot (2016).

percontinent demonstrates an unstable climate at this insolation and outgassing, suggesting a strong sensitivity to continental distribution that requires further investigation.

IV. SIMULATION CAVEATS

While PlaSim represents a model of much greater complexity than the simplified model used in Menou (2015), it does have limitations. The radiation model used in PlaSim is highly simplified, largely ignoring aerosols and finer spectral variations in absorptivities, relying on broadband emissivities, polynomial prescriptions, and constant albedos, and insufficiently treating the stratosphere, resulting in biases (Lunkeit et al. 2012). For example, different models can predict significantly different cooling rates for a given T - $p\text{CO}_2$ combination, resulting in different abundances and durations of snowball states. Williams & Kasting (1997, hereafter WK97) ran a suite of 1D models for various $p\text{CO}_2$ levels, and then fit polynomials to the radiative results of the models. They claim an rms error in outgoing longwave radiation (OLR) of less than 5 W/m^2 in the 190–370 K temperature range and from 10^{-5} –10 bars pressure range. Almost all of our models fall within this $p\text{CO}_2$ range. We compute a global annual mean of outgoing longwave (thermal) radiation by recording the outgoing longwave radiation (OLR) at each grid point 4 times per simulated day. We then compare this with the OLR predicted by the WK97 polynomial fit assum-

Warm Period (Zoomed in), $V_{\oplus}=7$ bar/Gyr

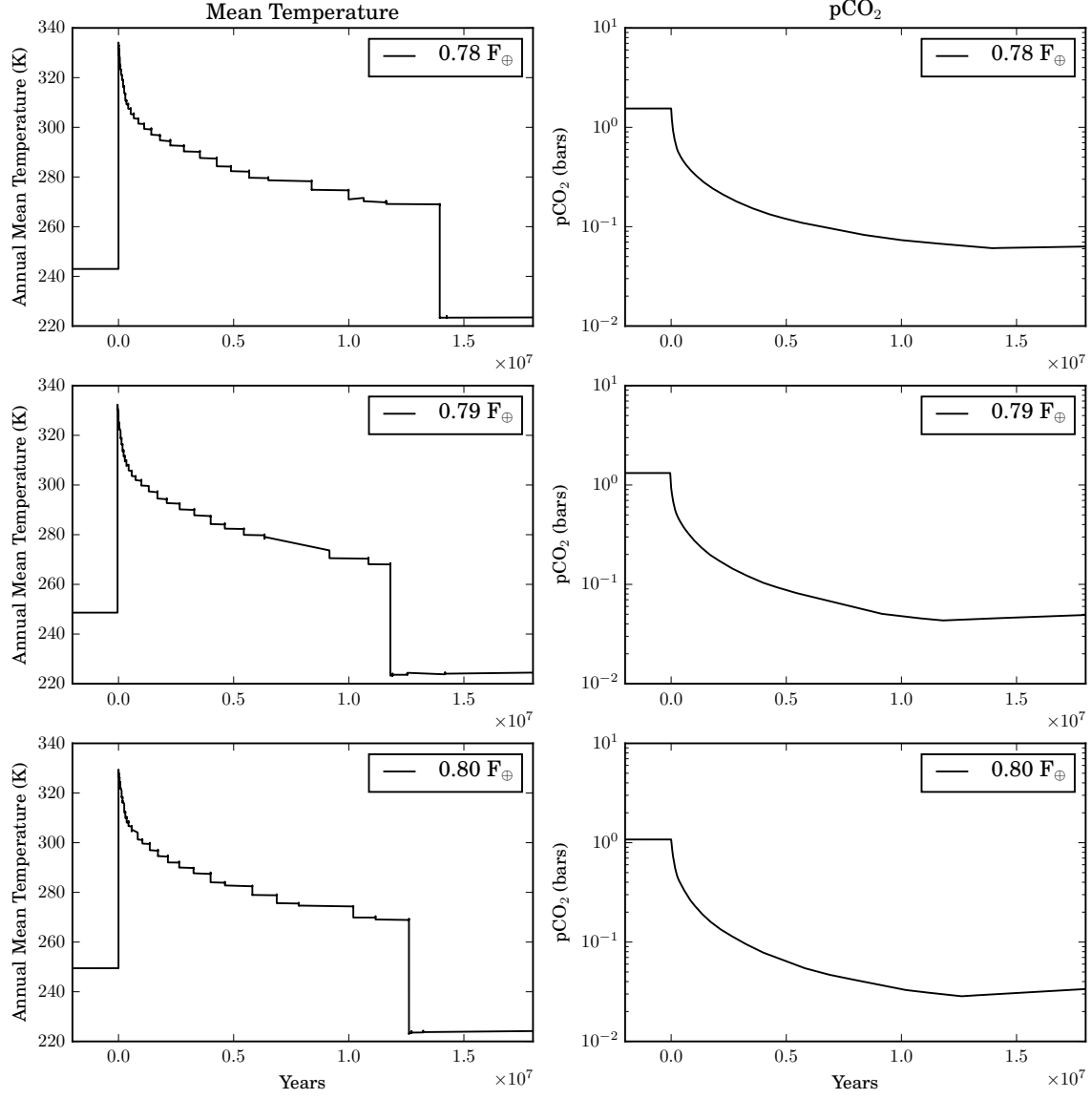


Figure 4. The warm periods of the cycles shown in Figure 3. These periods last on the order of 10–15 Myr. Note that much of the cooldown and reduction in pCO₂ happens rapidly, with the climate’s rate of change slowing dramatically until a tipping point is reached. The cooldown during the temperate phase involves nonlinear and highly local sea ice effects, but because it occurs on Myr timescales, still requires only intermittent GCM steps. Compared to the relatively uneventful snowball outgassing phase, capturing enough of the nonlinearity to describe the cooldown requires striking a balance between time-sampling resolution and computational expense. This balance between feasibility and nonlinear response is responsible for the seemingly discontinuous jumps in the temperature—each jump represents a decade- or century-scale GCM relaxation step.

Plasim Cooling Rates vs WK97 at 1 AU

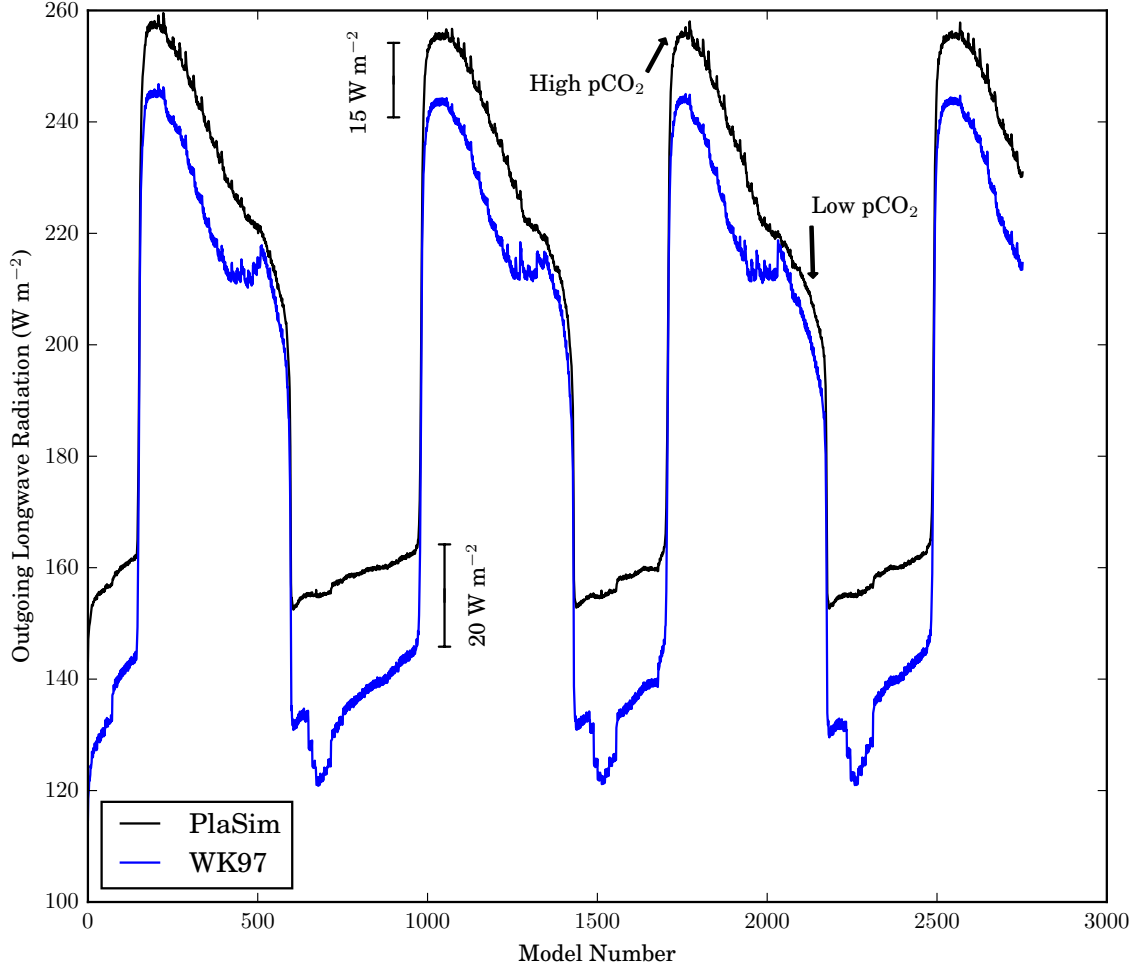


Figure 5. Comparison of outgoing longwave radiation (OLR) throughout cycles at 1 AU and mbar Gyr^{-1} outgassing as computed by PlaSim, and as computed by the polynomial fit proposed by Williams & Kasting (1997). Each model number is one GCM year. We compute the WK97 polynomial by computing the global average surface temperature over the 3D GCM outputs, and compute a single polynomial with that and pCO_2 as input. The two models predict global cooling rates that can differ significantly in the high- pCO_2 regime, by up to tens of percent. This suggests substantial uncertainty in the quantitative abundance and duration of limit cycles in the habitable zone.

ing the same global annual surface temperature and pCO_2 , computing a single polynomial with the global values as inputs. The comparison is shown in Figure 5. PlaSim consistently predicts more cooling, by 10% or less during warm phases, but by up to 70% in the frozen phase. Even in a best-case scenario of Earth insolation, using 1 mbar Gyr^{-1} outgassing to trigger limit cycles, PlaSim predicts more cooling. Thus, without repeating this study with different GCMs, our results cannot be considered quantitative predictions for where climate cycles might occur beyond identifying a general trend—we expect limit cycles to

dominate the outer habitable zone, with a boundary roughly described by an exponential trend, as in [Equation 5](#).

The carbon-silicate cycle implementation is itself a simplification, limited by parameterizations of Earth weathering, and ignoring sea-floor weathering or mantle CO₂ processes. One important simplification is in precipitation and runoff. [Equation 1](#) includes a term that depends on runoff efficiency and temperature. This is intended to account for changes in precipitation and runoff and the resulting effect on weathering ([Abbot et al. 2012](#)). However, this may miss complexities arising from glacial melt and changes in the hydrologic cycle due to large changes in ice fraction. As ice sheets advance to the equator, the amount of precipitable water present in the atmosphere is expected to dramatically decline, leading to a reduction in weathering due to precipitation and runoff. Our implementation also involves computing what was originally a global, 0D parameterization at each grid point and then taking the average, rather than taking into account such variables as the precipitation specific to that gridpoint. It is important to note that we are effectively taking the average of a polynomial, rather than computing a polynomial with an average input. A more sophisticated weathering model might yield quantitatively different results when used with our long-time evolution technique. Nor do we consider the impact of CO₂ condensation on weathering feedbacks. [Turbet et al. \(2017\)](#) showed that snowball states at low insolation may result in large amounts of CO₂ deposition as dry ice at the planet’s pole. We ignore the effect that could have on limit cycles.

PlaSim also neglects glacial dynamics—instead, snow simply accumulates on land. This means that glacial flow is ignored, and any differences in albedo or melting properties between large accumulations of snow and glaciers are ignored. This could produce qualitatively different results in how the planet melts and freezes. We also ignore any interaction between glaciation and volcanism. There likely is some important interaction, as some studies suggest that rapid changes in lithostatic pressure due to rapid melting could trigger volcanic activity ([Sternai et al. 2016](#)), and others suggest that increased lithostatic pressure on continents due to glacial loading could also trigger volcanic activity ([Kyle et al. 1981](#)). The amount of volcanic activity will also have an effect on snow and ice albedo by changing the amount of soot and other contaminants in the snow and ice ([Gow & Williamson 1971](#)).

Our models also do not take into account changes in sea level due to melting or freezing. As weathering rate depends on land fraction, this may have a significant impact. We also do not fully-treat large-scale ocean circulation, which tends to discourage the advance of sea ice, as currents transport heat away from the equator ([Poulsen et al. 2001](#)). We also ignore variations in fundamental orbital properties such as stellar luminosity and secular variations in the orbit itself, both of which can be expected to vary on relevant timescales ([Greenberg & Van Laerhoven 2011](#); [Gómez-Leal et al. 2016](#)).

The result of these caveats is that fully modeling a planet with any predictive accuracy is difficult, requires a great deal of physics and computation, and suggests both breadth and diversity in the habitable zone exoplanet parameter space. However, by limiting the

investigation to a particular slice of that parameter space, we may investigate the effects of a particular mechanism on climate. Our results suggest that the carbon-silicate feedback mechanism permits climate cycles at low insolations and moderate-to-low outgassing rates, in general agreement with the results of [Tajika \(2007\)](#), [Menou \(2015\)](#), and [Haqq-Misra et al. \(2016\)](#). Our results are also consistent with the conclusions of [Batalha et al. \(2016\)](#) that limit cycles may have been important in the climate of early Mars due to low outgassing and low insolation, although our work does not probe insolations lower than those experienced by early Earth.

V. CONCLUSION

We present a technique for simulating the evolution of climate systems on geological timescales by using a 3D GCM as a relaxation step in a 0D carbon evolution model. We use this to present the first 3D GCM simulations of the climate cycles predicted by 1D models in [Menou \(2015\)](#) and [Haqq-Misra et al. \(2016\)](#). We find that Earth analogs undergo climate cycles at moderate outgassing levels and low insolations comparable to early Earth. Generally speaking, our findings are consistent with the proposal in [Batalha et al. \(2016\)](#) that early Mars may have been subject to limit cycles, as well as the hypothesis that Earth may have been subject to such episodes in its youth ([Tajika 2007](#)). Further work includes refining the model assumptions, accounting for other physical processes such as glacial dynamics, seafloor weathering ([Haqq-Misra et al. 2016](#)), and variable outgassing rates in response to glacial loading. We note that our technique is not specific to PlaSim, and any GCM could be used in its place using the same technique. We also note that we have not mapped the entirety of the parameter space proposed by our models to exhibit climate cycles; we have only probed a few points in that space to find climate cycles. Future work should map the cycle frequencies and characteristics in this region and compare with the results presented in [Menou \(2015\)](#), [Haqq-Misra et al. \(2016\)](#), and [Abbot \(2016\)](#). It may be additionally useful to explore more sophisticated weathering models which are truly 3D, rather than merely using a 3D temperature field to compute a global average weathering rate.

VI. ACKNOWLEDGMENTS

AP is supported by a Centre for Planetary Sciences Graduate Fellowship at the University of Toronto, Scarborough, and by the Department of Astronomy & Astrophysics at the University of Toronto, St. George. KM is supported by the Natural Sciences and Engineering Research Council of Canada. Computing time was provided by the Canadian Institute for Theoretical Astrophysics at the University of Toronto, St. George. Many thanks are given to my peers for their support.

Software: PlaSim (Fraedrich et al. 2005), matplotlib (Hunter 2007)

APPENDIX

A. COMPUTATIONAL COST

Earth-system general circulation models are often very computationally expensive. PlaSim is one of the faster GCMs available. On a compute node with two Intel® Xeon® E5310 quad-core CPUs, clocked to 1.60 GHz, running PlaSim in parallel with 8 threads takes 162 seconds of wall-time on average per simulated year, where wall-time is the real time that a user must wait for a job to finish. On a compute node with 2 octa-core Intel® Xeon® E5-2640 CPUs, clocked at 2.00 GHz, running PlaSim in parallel with 16 threads takes 62 seconds of wall-time on average per simulated year. Overall, PlaSim takes approximately 1300 CPU-seconds per simulated year on the E5310 cores and 1000 CPU-seconds per simulated year on the E5-2640 cores. As an example of a more sophisticated GCM, the ROCKE-3D Earth GCM developed at the NASA Goddard Institute for Space Studies can compute a simulated year in as little as 11 CPU-hours (38,000 CPU-seconds) on their Xeon® E5-2697 nodes using 44 cores (Way et al. 2017). Climate cycles, as proposed by Menou (2015), occur on the order of hundreds of millions of years to billions of years. Taking as an optimal computing case, if we assume a climate cycle could be found which lasts only 100 Myr, then on the computing hardware available to us, computing the entire cycle directly year-by-year with PlaSim on 16 cores would take 6.2×10^9 seconds of wall-time, or approximately 196 years. Since submitting a computing job with a run-time of two centuries is not practical or desirable, directly simulating the carbon-silicate cycle with a GCM is impossible without considerable computing resources. Our technique, however, allows us to avoid directly computing each year of climate evolution, at the cost of computational accuracy. Instead, we compute only a few decades intermittently throughout the long-term evolution of the planet. Computing two periods of the cycles observed in this paper involved directly simulating approximately 1800 years, which is 6 orders of magnitude less than directly computing the entire cycle, and allows full computation in only 31 hours of wall-time on our hardware.

REFERENCES

- | | |
|--|---|
| Abbot, D. S. 2016, <i>The Astrophysical Journal</i> , 827, 117 | Edson, A. R., Kasting, J. F., Pollard, D., Lee, S., & Bannon, P. R. 2012, <i>Astrobiology</i> , 12, 562 |
| Abbot, D. S., Cowan, N. B., & Ciesla, F. J. 2012, <i>ApJ</i> , 756, 178 | Fraedrich, K., Jansen, H., Kirk, E., Luksch, U., & Lunkeit, F. 2005, <i>Meteorologische Zeitschrift</i> , 14, 299 |
| Batalha, N. E., Kopparapu, R. K., Haqq-Misra, J., & Kasting, J. F. 2016, <i>Earth and Planetary Science Letters</i> , 455, 7 | Gómez-Leal, I., Codron, F., & Selsis, F. 2016, <i>Icarus</i> , 269, 98 |
| Berner, R. a. 2001, <i>American Journal of Science</i> , 301, 182 | Gow, A. J., & Williamson, T. 1971, <i>Earth and Planetary Science Letters</i> , 13, 210 |
| Budyko, M. I. 1969, <i>Tellus</i> , 21, 611 | |

- Greenberg, R., & Van Laerhoven, C. 2011, *ApJ*, 733, 8
- Haqq-Misra, J., Kopparapu, R. K., Batalha, N. E., Harman, C. E., & Kasting, J. F. 2016, *ApJ*, 827, 120
- Hoffman, P., Kauffman, A., Halverson, G., & Schragg, D. 1998, *Science*, 281, 1342
- Hunter, J. D. 2007, *Computing In Science & Engineering*, 9, 90
- Kopparapu, R., Ramirez, R., Kasting, J., et al. 2013, *The Astrophysical Journal*, 765, 131
- Kump, L., Brantley, S., & Arthur, M. 2000, *Annual Review of Earth and Planetary Sciences*, 28, 611
- Kyle, P. R., Jezek, P. A., Mosley-Thompson, E., & Thompson, L. G. 1981, *Journal of Volcanology and Geothermal Research*, 11, 29
- Lunkeit, F., Borth, H., Böttinger, M., et al. 2012, *Planet Simulator Reference Manual*, 16th edn., National Center for Atmospheric Research
- Menou, K. 2015, *Earth and Planetary Science Letters*, 429, 20
- North, G., Cahalan, R., & Coakley, Jr, J. 1981, *Reviews of Geophysics and Space Physics*, 19, 91
- Pierrehumbert, R. 2005, *Journal of Geophysical Research*, 110, 1
- . 2010, *Principles of Planetary Climate* (Cambridge University Press)
- Poulsen, C. J., Pierrehumbert, R. T., & Jacob, R. L. 2001, *Geophys. Res. Lett.*, 28, 1575
- Schwartzman, D., & Volk, T. 1989, *Nature*, 340, 457
- Sternai, P., Caricchi, L., Castelltort, S., & Champagnac, J.-D. 2016, *Geophysical Research Letters*, 43, 1632, 2015GL067285
- Tajika, E. 2007, *Earth, Planets, and Space*, 59, 293
- Turbet, M., Forget, F., Leconte, J., Charnay, B., & Tobie, G. 2017, 1
- Walker, J., Hays, P., & Kasting, J. 1981, *Journal of Geophysical Research*, 86, 9776
- Way, M. J., Aleinov, I., Amundsen, D. S., et al. 2017, *ArXiv e-prints*, arXiv:1701.02360
- Williams, D. M., & Kasting, J. F. 1997, *Icarus*, 129, 254